ARL-TR-9714 ● JUNE 2023

Property Estimates for Hydroxyl-Terminated Polybutadiene (HTPB) Type R45M Derived from Atomistic Molecular Dynamics Simulations

by Jeffrey D Veals, Chiung-Chu Chen, In-Chul Yeh, Christopher P Stone, Michael J McQuaid, and Claresta Dennis

NOTICES

Disclaimers

The findings in this report are not to be construed as an official Department of the Army position unless so designated by other authorized documents.

Citation of manufacturer's or trade names does not constitute an official endorsement or approval of the use thereof.

Destroy this report when it is no longer needed. Do not return it to the originator.

ARL-TR-9714 ● JUNE 2023

Property Estimates for Hydroxyl-Terminated Polybutadiene (HTPB) Type R45M Derived from Atomistic Molecular Dynamics Simulations

Jeffrey D Veals, Chiung-Chu Chen, In-Chul Yeh, Christopher P Stone, and Michael J McQuaid
DEVCOM Army Research Laboratory

Claresta Dennis
Naval Air Warfare Center Weapons Division (NAWCWD)

REPORT DOCUMENTATION PAGE

1. REPORT DATE	2. REPORT TYPE	3. DATES COVERED	
		START DATE	END DATE
June 2023	Technical Report	1 June 2022	31 May 2023

4. TITLE AND SUBTITLE
Property Estimates for Hydroxyl-Terminated Polybutadiene (HTPB) Type R45M Derived from Atomistic Molecular Dynamics Simulations

5a. CONTRACT NUMBER	5b. GRANT NUMBER	5c. PROGRAM ELEMENT NUMBER
5d. PROJECT NUMBER	**5e. TASK NUMBER**	**5f. WORK UNIT NUMBER**

6. AUTHOR(S)
Jeffrey D Veals, Chiung-Chu Chen, In-Chul Yeh, Christopher P Stone, Michael J McQuaid, and Claresta Dennis

7. PERFORMING ORGANIZATION NAME(S) AND ADDRESS(ES)
DEVCOM Army Research Laboratory
ATTN: FCDD-RLA-WC
Aberdeen Proving Ground, MD 21005

8. PERFORMING ORGANIZATION REPORT NUMBER
ARL-TR-9714

9. SPONSORING/MONITORING AGENCY NAME(S) AND ADDRESS(ES)	10. SPONSOR/MONITOR'S ACRONYM(S)	11. SPONSOR/MONITOR'S REPORT NUMBER(S)

12. DISTRIBUTION/AVAILABILITY STATEMENT
DISTRIBUTION STATEMENT A. Approved for public release: distribution unlimited.

13. SUPPLEMENTARY NOTES
ORCID IDs: Jeffrey D Veals, 0000-0002-8238-345X; Chiung-Chu Chen, 0000-0002-8666-9949; Michael J McQuaid, 0000-0001-5523-7468; Christopher P Stone, 0000-0002-9621-5334

14. ABSTRACT
Seeking to parameterize models for simulating the deflagration of hydroxyl-terminated polybutadiene type R45M, we employed atomistic molecular dynamics (MD) methods to obtain estimates for some of R45M's transport and thermophysical properties. Estimates for densities, enthalpies of vaporization, and self-diffusion coefficients were derived from simulations of hydroxyl-terminated 6-ethenenyl-2,8,12,16-octadecatetraene (EODT, $C_{20}H_{32}$) oligomer systems. The dependencies of the predictions on the number of monomers per oligomer (n), system size, simulation temporal duration, and force-field type were evaluated. Comparisons to measured values indicate the predictions' merit. In addition, we coupled MD-based estimates for the HO–$(EODT)_n$–OH systems' enthalpies of vaporization with estimates for their gas-phase enthalpies to estimate R45M's enthalpy of formation and heat capacity as a function of temperature. The enthalpy of formation estimates at 298 K were observed to be in reasonable agreement with a recently published aggregation of such values. Heat capacity estimates were in reasonable agreement with values we measured. The potential to employ the self-diffusion coefficient predictions as a basis for parameterizing a theorized framework for modeling condensed-phase chemical kinetics is discussed.

15. SUBJECT TERMS
Weapons Sciences, propulsion, chemical kinetics, pyrolysis, molecular dynamics, free volume theory

16. SECURITY CLASSIFICATION OF:			17. LIMITATION OF ABSTRACT	18. NUMBER OF PAGES
a. REPORT	b. ABSTRACT	C. THIS PAGE		
UNCLASSIFIED	UNCLASSIFIED	UNCLASSIFIED	UU	44

19a. NAME OF RESPONSIBLE PERSON	19b. PHONE NUMBER *(Include area code)*
Michael J McQuaid	(410) 278-6185

STANDARD FORM 298 (REV. 5/2020)
Prescribed by ANSI Std. Z39.18

Contents

List of Figures

List of Tables

Acknowledgments

Funding for this study was primarily provided by the US Army Combat Capabilities Development Command Army Research Laboratory's Machine Learning to Accelerate Detailed Finite-Rate Chemical Kinetics Mechanism Creation for Continuum-Level Modeling of Energetic Material Decomposition and Combustion mission program. Dr Dennis was funded by an Office of Naval Research-sponsored program titled, "Detailed Investigation of Hydroxyl-Terminated Polybutadiene Combustion and Regression." The thermal transport properties of cured R45M were measured by Dr Thao Tran-Ngo (NAWCWD). The molecular dynamics simulations were performed on DOD High Performance Computing Modernization Program computing platforms.

1. Introduction

As part of a program to develop and validate a theorized framework for creating detailed finite-rate chemical kinetics mechanisms for modeling the condensed-phase reaction chemistry of energetic material (EM) formulations, we are investigating the potential of atomistic molecular dynamics (MD) methods to produce timely and cost-effective estimates for some of the framework's parameters. In essence an extension of the free-volume theory (FVT) of molecular transport in liquids and glasses (Cohen and Turnbull 1959), the framework predicates specifying rate coefficients (k_c^i) for elementary condensed-phase reactions (i) via the multiplication of their gas-phase analogs (k_g^i) by a function that estimates the probability (P) that reactants are adjacent to a free-volume hole large enough for a chemical reaction to proceed unhindered concomitant with a diffusive jump that prevents the reaction from reversing (Veals et al. 2018; McQuaid et al. 2021). That is,

$$k_c^i = P\left(\hat{V}_{hfv}\right)k_g^i, \tag{1}$$

where $\hat{V}_{hfv}$ is the medium's mean hole free volume.

As we have recounted previously (McQuaid et al. 2021), FVT posits that the self-diffusion coefficients (D) of "simple" liquids can be computed as a function of temperature (T) per

$$D(T) = AP\left(\hat{V}_{hfv}(T)\right) \tag{2}$$

where A is a system-specific constant and

$$P\left(\hat{V}_{hfv}(T)\right) = \exp\left(\frac{-\gamma\hat{V}^*}{\hat{V}_{hfv}(T)}\right) \tag{3}$$

where γ and $\hat{V}^*$ are constants related to molecular size. Naturally expressed per

$$P\left(\hat{V}_{hfv}(T)\right) = \exp\left(\frac{-B}{T-T_0}\right) \tag{4}$$

where B and T_0 are system-specific constants, a capacity to establish $D(T)$ values enables one to estimate B and T_0. Likewise, the relationship between D, viscosity (η), and density (ρ) predicted by the Stokes–Einstein equation

$$D(T) = A'\left(\frac{\rho(T)T}{\eta(T)}\right) \tag{5}$$

where A' is (again) a system-specific coefficient, offers a means for deriving B and T_0 from estimates for $\eta(T)$ and $\rho(T)$.

As a step toward evaluating this framework, we combined measurement-based $\eta(T)$ values from the 1930s (Peterson 1930) with $\rho(T)$ estimates derived from atomistic MD simulations to parameterize $P(\hat{V}_{hfv})$ for nitroglycerin (NG_l) and four other nitrate esters that are liquids (l) at 298 K and 1 atm (McQuaid et al. 2021). The $P(\hat{V}_{hfv})$ derived in this manner appeared to be reasonable, and the function for NG_l was subsequently integrated into a homogeneous reactor (HR) model for simulating NG_l's decomposition in two-phase NG_g–NG_l systems (McQuaid et al. 2021). Predictions for the global rate of NG's decomposition produced by the baseline/a priori model proved to be about a factor of 10 lower than values measured by Waring and Krastins (1970). However, from a thermodynamics standpoint, the corrections needed to bring the results into agreement were small, and the model yielded insight into the process that led to a more compelling and self-consistent explanation for Waring and Krastins' results.

Although encouraged by that success, we assumed the application of the methodology would be extremely limited if it had to rely on measurement-based $\eta(T)$ values to parameterize $P(\hat{V}_{hfv})$. Therefore, we investigated the use of atomistic MD methods to estimate $\eta(T)$ for the five nitrate esters for which Peterson (1930) had measured values (Veals et al. 2018). Results were mixed. Trends in the $\eta(T)$ predictions for the nitrate esters were consistent with Peterson's measurement-based values. However, there were significant discrepancies between the magnitudes of the predicted and measured $\eta(T)$ values, and the discrepancies increased with increasing $\eta(T)$. Thus, we were concerned about the capacity of MD-based methods to produce reliable $\eta(T)$ estimates for polymeric/solid materials.

The need to parameterize $P(\hat{V}_{hfv})$ for hydroxyl-terminated polybutadiene (HTPB) type R45M arose while developing and applying a model to represent its pyrolysis (McQuaid et al. 2023). Uncured R45M prepolymer is a relatively low-viscosity liquid (5000–8000 centipoise at 303 K) and its ρ is approximately 0.90 g/cm^3 at 298 K and 1 atm. Curable to various degrees of solidification, capable of taking solid loadings up to 86%–88% without sacrificing the ease of processibility (Muthiah et al. 1992), having a relatively low glass-transition temperature (T_g), high tensile strength, and being chemically compatible with nitramines and ammonium perchlorate at normal storage conditions (Eroglu 1998; Mahanta 2012), R45M is widely used as a binder in EM formulations (Armado et al. 2022; Chen and McQuaid 2009, 2020).

With respect to parameterizing $P\left(\hat{V}_{hfv}(T)\right)$ for R45M, the situation appeared to be more complicated than it was in the case of the nitrate esters. Since the nitrate esters were (to our minds) "simple" liquids, the self-diffusion coefficients of reactants and products in them could be assumed to be similar to the parent molecule's. Therefore, parameterizations based on the properties of the neat liquid alone were considered sufficient for that purpose.

Extending FVT to explain differences in the diffusional behavior of solvents in amorphous polymers, Vrentas and Duda (1977a,b) posited that the self-diffusion coefficient of a solvent (D_1) in an amorphous polymer was related to the mixture's $\hat{V}_{hfv}$ per

$$D_1(T) = D_{01}\exp\left[\frac{-(\omega_1\hat{V}_1^{*}+\xi\omega_2\hat{V}_2^{*})}{\hat{V}_{hfv}/\gamma}\right] exp\left[\frac{-E_{D1}}{RT}\right] \qquad (6)$$

where the subscripts 1 and 2 identify solvent and polymer properties, respectively. In this equation, D_{01} is a constant. ω_k is component k's mass fraction. $\hat{V}_k^*$ is the specific critical hole free volume that k's "jumping unit" needs to make a diffusive jump. γ is an overlap factor included to account for the fact that more than one jumping unit may have access to a hole. ξ is a function of $\hat{V}_1^*$, $\hat{V}_2^*$, and the molecular weights (*M* values) of the solvent and the jumping unit. E_{D1} is the energy needed for a solvent molecule to overcome the attractive forces that bind it to its neighbors.

Interested in making Eq. 6 "predictive," Zielinski and Duda (1992) proffered methods for estimating all its parameters without any diffusion data. They assumed $\hat{V}_1^*$ and $\hat{V}_2^{*}*$ could be set equal to group-contribution-based estimates for the specific volumes of the jumping units at 0 K. And for small molecules, ξ could be derived from those estimates and the molecules' *M* values. Finding $\hat{V}_{hfv}/\gamma$ expressible per

$$\hat{V}_{hfv}/\gamma = \omega_1\frac{K_{11}}{\gamma}\left(K_{21}+T-T_{g1}\right)+\omega_2\frac{K_{12}}{\gamma}\left(K_{22}+T-T_{g2}\right), \qquad (7)$$

they established six other parameters that needed to be estimated to complete the parameterization: D_{01}, E_{D1}, K_{11}/γ, $(K_{21}-T_{g1})$, K_{12}/γ, and $(K_{22}-T_{g2})$. (All correspond to physical properties.) For estimating the polymer properties K_{12}/γ and $(K_{22}-T_{g2})$, one suggestion was to fit the (re-casted) Doolittle (1951) expression

$$\eta_2(T) = A_2 exp\left[\frac{\gamma\hat{V}_2^{*}/K_{12}}{(K_{22}-T_{g2})+T}\right] \qquad (8)$$

where A_2 is a constant, to measured $\eta_2(T)$ values.

Derived empirically prior to FVT, Doolittle's expression is identical in form to the right-hand side of Eq. 4 (times a constant), suggesting $\gamma \hat{V}_2^*/K_{12} = B$ and $\left(K_{22} - T_{g2}\right) = T_0$. However, in contrast to Eq. 5, it indicates that the influence of T and $\rho(T)$ on the relationship between $D_2(T)$ and $\eta_2(T)$ is negligible. We did not appreciate this fact until this report was being written. For establishing the relationship between $D(T)$ and $\eta(T)$ for NG*l*, we had followed Zielinski and Duda's (1992) protocol for establishing the relationship between $D_1(T)$ and $\eta_1(T)$ (for solvents). That protocol employed a variation of Eq. 5 recommended by Dullien (1972). As such, it was clear that Zielinski and Duda's use of Eq. 8 for polymers was not an oversight or a matter of convenience. Although ρ values tend to decrease with an increase in T, and their product can therefore be expected to be less than directly proportional to T, there is likely to be some *T*-dependence; Zielinski and Duda did not discuss this matter. It is considered further in Section 4.

Unaware of that issue, we sought to demonstrate that a fit of Eq. 4 (times a constant) to MD-based $D(T)$ estimates would produce reliable estimates for B and T_0. As will be appreciated by consideration of Eq. 6, for a "pristine" polymer—that is, no impurities meaning all ω_1 are 0 – $D_1(T)$ will equal $D_2(T)$ and thus should produce a $P\left(\hat{V}_{hfv}\right)$ that is applicable for modeling the onset of R45M's decomposition.

Relevant to this study, several atomistic MD and coarse-grained dissipative particle dynamics (CG-DPD) modeling studies have been performed to characterize bulk and/or viscoelastic properties of R45M and related polybutadiene polymers. Notably, in a recent study published by Dossi et al. (2021), the general-purpose Dreiding force field was employed as the basis for atomistic MD simulations designed to explore the T_g values and related properties of HTPB chains comprising either four or five butadiene (BD) monomers. The results suggested that the onset of glassy behavior in different HTPB systems at temperatures from 178 to 248 K is predicted by vinyl content; an increase in it decreases the frequency of crankshaft shifts of main chain sub-regions. Kempfer (2019) employed a CG-DPD model to estimate the properties of HTPB melts over a broad range of temperatures and pressures. He found that his CG-DPD model produced thermal expansion coefficients and isothermal compressibility values that were in reasonable agreement with measured values.

Herein we present atomistic MD-based property predictions for systems comprising hydroxyl-terminated oligomers of a notional molecule/monomer with the formal name 6-ethenenyl-2,8,12,16-octadecatetraene (EODT, $C_{20}H_{32}$). Employed by us to represent the nascent products of R45M's pyrolysis in deflagration scenarios (Chen and McQuaid 2009), EODT is roughly one-ninth the

size of nominal R45M polymer chains. Moreover, EODT has the same ratio of cis/trans/vinyl BD monomers as R45M's chains.

Because the accuracy/reliability of MD-based estimates depends on a number of factors whose specifications are constrained by computational costs, including force-field type/complexity, system size, monomers/oligomer (n), and simulation duration, we performed a parametric study to establish the impact of each on predictions for $D(T)$ and $\rho(T)$ (or specific volume $V(T) = \rho(T)^{-1}$). Comparisons with the limited number of measurement-based $D(T)$ values for similar systems indicate the merit of the MD-based estimates for unentangled polymers. In addition, a $P\left(\hat{V}_{hfv}(T)\right)$ parameterization based on the predictions proved to be in reasonable agreement with one based on measured $\eta(T)$ values. As such, the study suggested that MD-based methods hold promise for parameterizing $P\left(\hat{V}_{hfv}(T)\right)$ for notional polymeric EM ingredients.

In addition, cognizant of the uncertainty in the value of R45M's (condensed-phase) enthalpy of formation as a function of temperature [$\Delta_f H_c(T)$] (McQuaid 2020; Thomas and Petersen 2022) and that property being an important parameter in models for predicting its linear deflagration rate (Chen et al. 2019), we sought to exploit the MD-based results to obtain estimates. Specifically, MD-based estimates for HO–(EODT)$_n$–OH system enthalpies of vaporization [$\Delta H_v(T)$] were subtracted from gas-phase enthalpy-of-formation [$\Delta_f H_g(T)$] estimates for the corresponding oligomer that were derived from quantum mechanics-based electronic structure methods (QM-ESMs). Comparisons to values obtained by other means indicate their merit.

2. Experimental Methods

A cold properties viscometer (Anton Parr SVM 3001) was used to determine the $\eta(T)$ and $\rho(T)$ of Poly bd* R45M at temperatures from 323 to 408 K in 5-K increments. Measurements at each temperature set point were repeated seven times. In addition to these measurements, data was obtained during temperature soaks at 323 and 373 K. At each temperature, the sample cell was held at the set point for 60 min and measurements were obtained at 15-min increments. No substantial change in properties was observed, indicating the sample did not decompose.

Thermal transport properties of R45M cured with IPDI to an NCO/OH ratio of 1.0 were measured using a transient plane source (HotDisk TPS 2200). This instrument has a combined heat source and temperature probe that is placed between two

* Poly bd is a registered trademark of Cray Valley USA, LLC.

samples. Samples were heated with a discrete power pulse for a specified time interval and the resulting temperature response recorded. Heat capacity and thermal diffusivity were calculated on the basis of the response. The instrument was calibrated using NIST-traceable samples of stainless steel. Measurements were obtained at temperature set points from 263 to 413 K. Four separate measurements were made at each set point.

3. Computational Methods

The MD simulations were performed with the Large-scale Atomic/Molecular Massively Parallel Simulator (LAMMPS) (Plimpton 1995). Force fields included the Class-II types PCFF and COMPASS. PCFF was originally developed to study common organic polymers (Sun 1994). COMPASS is effectively an extension of PCFF that includes atom types whose parameters have been optimized to produce reliable potential energy predictions for the relatively unique electronic and structural properties of energetic functional groups (Sun 1998; Bunte and Sun 2000; McQuaid et al. 2004). Because the HO–(EODT)$_n$–OH systems did not contain any such functional groups, COMPASS was not necessarily needed for this study. However, anticipating that COMPASS will likely be employed for future MD-based studies of EMs, we were interested in how it would perform.

3.1 Simulation Setup and Protocols

Figure 1 presents an overview of the MD methods and protocols employed for this study. The Enhanced Monte Carlo (EMC) tool (in 't Veld and Rutledge 2003) was employed to create and pack HO–(EODT)$_n$–OH (n = 1, 2, 3, 4, 5, 8, or 10) chains (Fig. 2) into cells. It employed a Monte Carlo algorithm to build the chains. The PCFF force field as implemented in EMC was the basis for generating intramolecular bond lengths and angles.

To establish the system sizes (i.e., number of atoms/cell) beyond which estimates for the properties of interest converged, two cells were built for each n-omer: one comprising approximately 5,000 atoms and one comprising approximately 10,000 atoms (Table 1). In all cases, results produced by the two sizes proved to be similar, indicating the 10,000-atom systems were more than adequately large. Those results are reported herein.

To mitigate any excessively repulsive atom–atom interactions that the EMC-generated configurations might have had, an energy minimization and a short constant-temperature, constant-pressure ensemble (NPT) simulation were performed to reduce them.

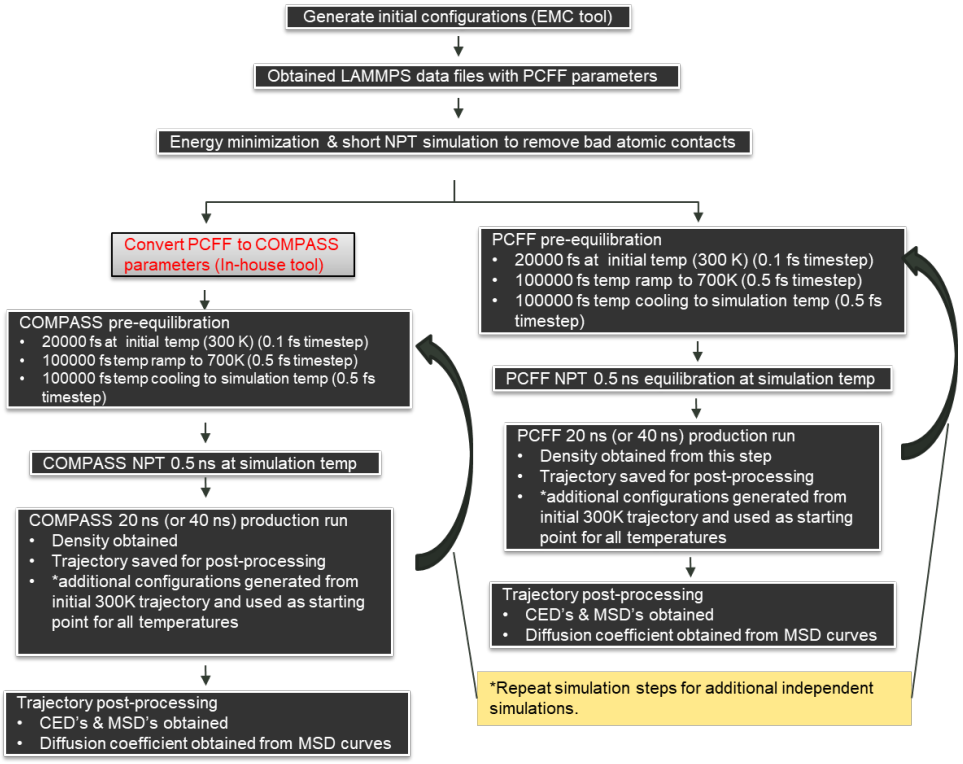

Fig. 1 Overview of MD methods and protocols employed to obtain property estimates. Note that after the conversion of PCFF parameters into COMPASS parameters the protocols were the same.

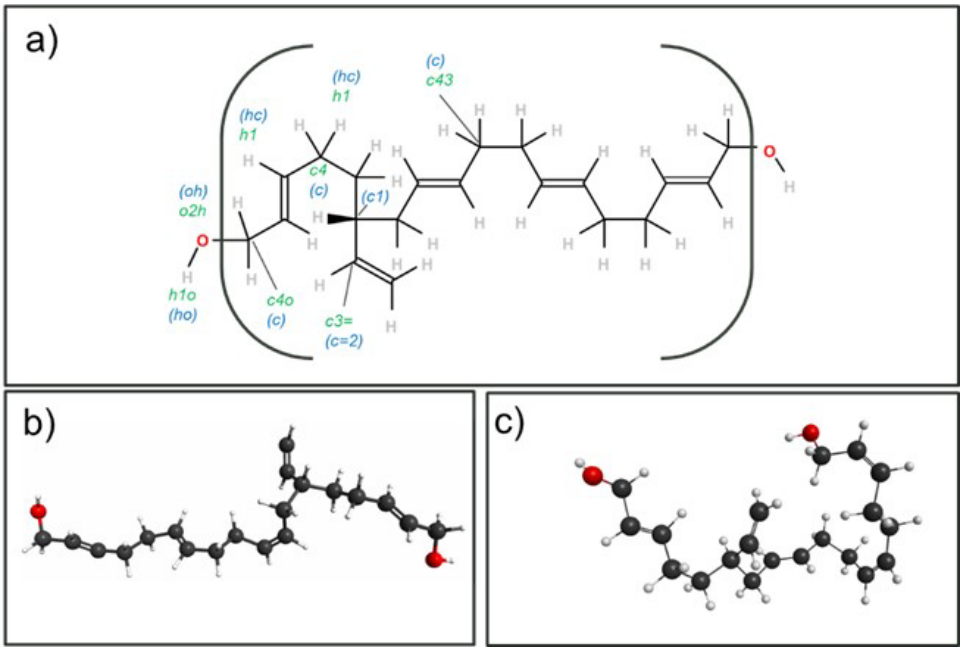

Fig. 2 The molecular structure of hydroxyl-terminated EODT oligomers: a) HO–(EODT)$_n$–OH (green and blue labels are for COMPASS and PCFF force-field atom types, respectively); b,c) two possible HO–EODT–OH conformers

Table 1 Number of atoms per system

n-omer	System A	System B
1	9990	5184
2	10192	5200
4	10200	5100
5	10160	5080
8	10100	4848
10	10080	5040

From the pre-equilibrated cells, the atomic coordinates, atom types, and the topology information (i.e., the atomic connectivity patterns and associated coefficients for all force-field potential energy terms) produced with the PCFF-based model were used to create starting configurations for COMPASS-based simulations. Because the COMPASS force field is intended for use with Materials Studio modules, to ensure that the force-field parameter conversions were valid, various LAMMPS-generated energy components—including total potential energy, bond energy, angle energy, and torsion energy—were compared to analogous energy components generated using Materials Studio's Forcite module.

Prior to performing production runs, the "pre-equilibrated" EMC-generated cells were more fully equilibrated via a sequence of four simulations. For these simulations (and the production runs), electrostatic interactions were calculated via an Ewald summation using the particle–particle particle–mesh (PPPM) method implemented in LAMMPS. Short-range van der Waals interactions within a 12.5 Å cutoff limit were calculated with 9-6 Lennard–Jones functions. Pressure was maintained at 1.01325 bar (1 atm) with a Nosé–Hoover barostat. Temperature was maintained at targeted temperatures with a Nosé–Hoover thermostat. The first simulation was a 0.02-ns NPT run at 300 K. The second was a 0.1-ns run in which the temperature was ramped to 700 K in (fixed) 0.5-fs time steps. The third was a 0.1-ns run in which the cell was cooled back to the target temperature in 0.5-fs time steps. That was followed by a 0.5-ns NPT run at the target temperature. Time steps were 1.0 fs.

The preproduction-run equilibration protocol was followed by a 20- or 40-ns NPT production run. The former duration was found to be sufficient for smaller (n = 1, 2 or 4) n-omers; the latter was required for larger (n = 5, 8, or 10) n-omers. Time steps were 1 fs. Relaxation times were 0.1 ps for the thermostat and 1.0 ps for the barostat. In each case, the target temperature for the first cell created was 303 K. Nuclear coordinates were saved every 10 ps.

To create additional unique/independent trajectories, 10 arbitrary frames were taken from the production run performed with the first cell, and they were processed

via the preproduction-run equilibration protocol. The temperatures of subsequent production runs were 323, 348, 373, 398, 473, and 500 K. (In each case, the initial configuration was from a 300-K simulation, and temperature ramping and annealing steps were performed prior to the production run at a given temperature.)

3.2 Self-diffusion Coefficients

As discussed by Maginn et al. (2019), one of the two commonly employed theoretical bases for deriving D estimates from MD simulations is the "Einstein" equation

$$D = \frac{1}{2d_\alpha N} \lim_{t \to \infty} \frac{\langle |\boldsymbol{r}(t) - \boldsymbol{r}(0)|^2 \rangle}{\mathrm{d}t} \tag{9}$$

where d_α is the number of dimensions, N is the number of particles, and $\langle |\boldsymbol{r}(t) - \boldsymbol{r}(0)|^2 \rangle$ is the mean square displacement (MSD) of the particles' positions $[\boldsymbol{r}(t)]$ at a given time (t) compared to their starting positions $\boldsymbol{r}(0)$. Because Eq. 9 predicates computing D values on the basis of MSDs in the limit "$t \to \infty$", we had assumed that estimates would improve with an increase in simulation duration. However, Maginn et al. (2019) recommended that they be calculated based on results in a "diffusive regime" corresponding to a "middle" temporal interval in the simulations. However, they were unaware of any objective approach to defining such an interval, stating only that the relationship between MSD and t should be approximately linear, and therefore would be characterized by ln(MSD) versus ln(t) plots that had slopes approximately equal to 1.

Offering no objective guidance for how long the simulations needed to be—only that they be long enough to include a region in which the slopes of ln(MSD) versus ln(t) plots were approximately equal to 1—we ran simulations of varying length to establish durations (t_d) in which MSD versus t plots for c3= atom types (COMPASS) or the c=2 atom types (PCFF) in the range $0.25t_d \leq t \leq 0.50t_d$ $(t_0 \leq t \leq t_{max})$ were reasonably well fit to a linear function:

$$\mathrm{MSD}(t) = m(t - 0.25t_d)^{n'=1} + b' \tag{10}$$

where m and b' were constants. The actual value of n' was obtained by fitting

$$\ln(\mathrm{MSD}(t) - b') = \ln(m) + n' \ln(t - 0.25t_d) \tag{11}$$

to the data in the interval. With d_α= 3, the substitution of m into Eq. 9 yields,

$$D = \frac{m}{6N}. \tag{12}$$

3.3 Thermodynamic Properties

Toward obtaining $\Delta_f H_c(T)$ estimates for the systems, we coupled MD-based $\Delta H_v(T)$ estimates with QM-ESM-based $\Delta_f H_g(T)$ estimates. The $\Delta H_v(T)$ estimates were derived from MD-generated cohesive energies (E_{coh}). Defined as the average intermolecular non-bond energy per mole (Barton 1991), $E_{coh}(T)$ is related to a material's $\Delta H_v(T)$ per,

$$\Delta H_v(T) \approx E_{coh}(T) + RT \tag{13}$$

where R is the universal gas constant.

The $\Delta_f H_g(T)$ estimates were obtained by calculating enthalpies of reaction for (hypothetical) isodesmic reactions. A summary of these calculations is provided in the Appendix. For HO–EODT–OH, we were able to obtain estimates on the basis of the full suite of QM-ESMs we normally employ for that purpose. They included CBS-QB3 (Montgomery et al. 2000), G3MP2B3 (Baboul et al. 1999), B3LYP (Becke 1993), MPWB95 (Becke 1996), M062X (Zhao and Truhlar 2008), BHandHLYP (Becke 1993), and DFTBA (Zheng et al. 2007) models. All were implemented via the GAUSSIAN 16 software package (Frisch et. al. 2016). For larger oligomers, some of these methods proved to be computationally intractable. And for the largest oligomers, only BHandHLYP/6-31G(d) and DFTBA models proved viable. However, comparisons of the results produced for smaller oligomers by these two models and (generally) more reliable ones suggested the former were an adequate basis for computing $\Delta_f H_g(T)$ estimates.

4. Results and Discussion

Figure 3 compares frames from NPT simulations for HO–EODT–OH and HO–(EODT)$_{10}$–OH systems that are representative of the two cases. Having shorter chains and higher OH content (and thus a greater potential for intermolecular hydrogen bonding), the former packed better, resulting in less free volume. As will be discussed, trends in the property estimates derived from the simulations for HO–(EODT)$_n$–OH systems can largely be rationalized based on that observation.

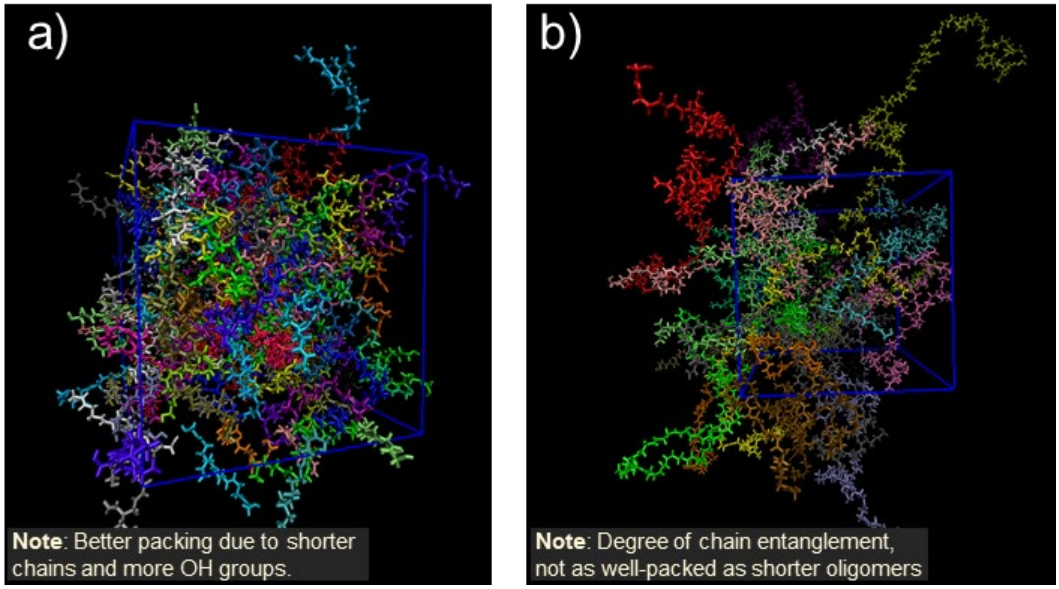

Fig. 3 Selected frames from NPT simulations: a) HO–EODT–OH and b) HO–(EODT)$_{10}$–OH

4.1 Density

Figure 4 shows ρ predictions for HO–(EODT)$_n$–OH systems at seven different temperatures between 303 and 500 K. The COMPASS-based predictions at 303 K ranged from 0.92 to 0.88 g/cm^3, decreasing as n increased from 1 to 10. We assume that trend was due to the smaller oligomer's potential to pack more efficiently (Fig. 3). Estimates produced by simulations involving approximately 5,000 atoms were very similar to those derived from their counterparts involving approximately 10,000 atoms, indicating that systems with about 5,000 atoms were large enough to yield good ρ predictions. The PCFF-based predictions exhibited similar trends. However, all PCFF-based predictions were slightly lower than their COMPASS-based counterparts at a given T. The differences ranged from 0.04 to 0.05 g/cc.

As shown in Table 2, the average of the COMPASS-based ρ predictions for HO–(EODT)$_8$–OH and HO–(EODT)$_{10}$–OH systems were in good agreement with measured values near 300 K and other COMPASS-based estimates for comparable systems. The PCFF-based predictions were less so. In addition, as shown in Fig. 5, the COMPASS-based estimates were in good agreement with values measured by us in the range 323 K $\leq T \leq$ 398 K. The PCFF-based ρ estimates exhibited similar trends as a function of T, but the estimates for all n-omer systems were below the measured values.

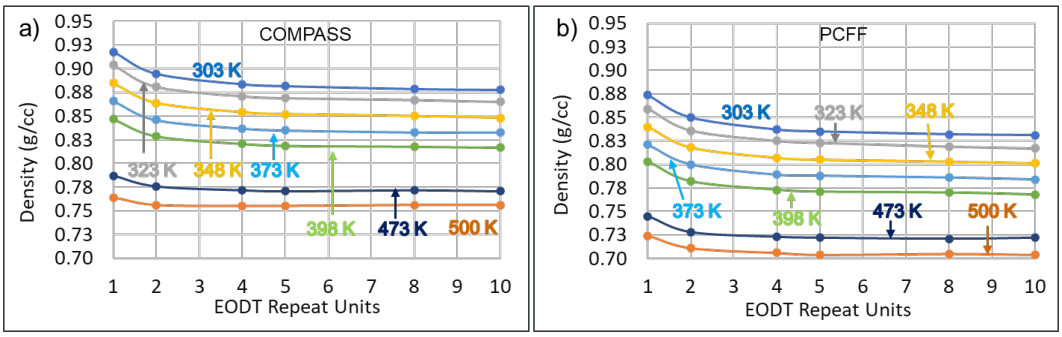

Fig. 4 COMPASS- and PCFF-based $\rho(T)$ estimates as a function of the number of EODT monomers/oligomer (n)

Table 2 Reference ρ values for HTPB near 300 K

ρ (g/cm³)		Reference
298 K	**303 K**	
. . .	0.88	COMPASS: Present work[a]
. . .	0.83	PCFF: Present work[a]
. . .	0.901	Measured: Lee et al. 2015
. . .	0.9	Measured: Mahanta 2012
. . .	0.902–0.904	Measured: Jabez et al. 2019
0.89 ± 0.04	. . .	COMPASS: Abou-Rachid et al. 2008
. . .	0.89–0.90	COMPASS: Yang et al. 2013

[a] Average of values derived from simulations involving HO–(EODT)$_8$–OH and HO–(EODT)$_{10}$–OH.

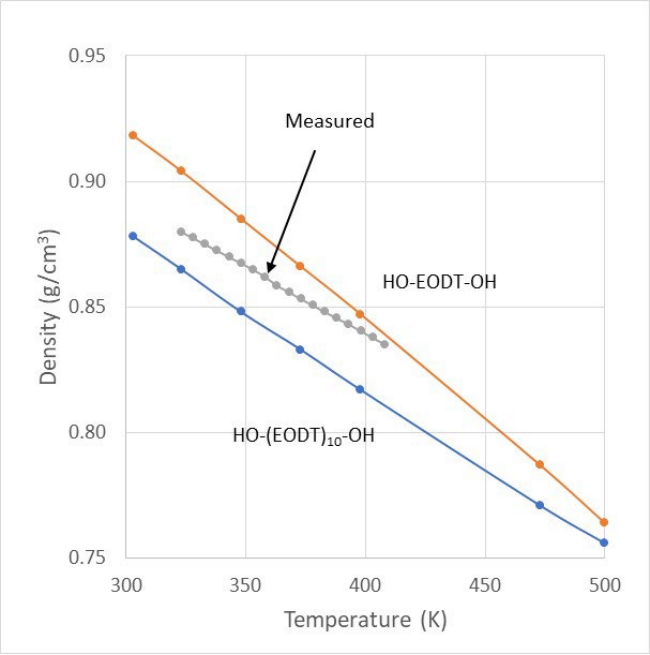

Fig. 5 COMPASS-based $\rho(T)$ predictions for HO–EODT–OH and HO–(EODT)$_{10}$–OH systems compared to measured values for R45M

4.2 Thermodynamic Properties

The $E_{coh}(T)$ and $\Delta H_v(T)$ estimates for the HO–(EODT)$_n$–OH systems are shown graphically in Fig. 6. As expected, they increased (on a molar basis) with increase in n. They also decreased with an increase in T. Given the reduction in ρ with increase in T, and thus an increase in the distance between sites with the potential to attract one another, that was also as expected.

Estimated $\Delta H_v(298)$ values are provided in Table 3. They demonstrate that the (molar) increase in $\Delta H_v(298)$ with increase in n was not quite linear, falling off at a rate somewhat lower than that (we presume) because packing efficiency declined with increase in n. The reduction in packing efficiency with increase in n is also reflected in the decrease in mass-specific $\Delta H_v(298)$ estimates as n increased.

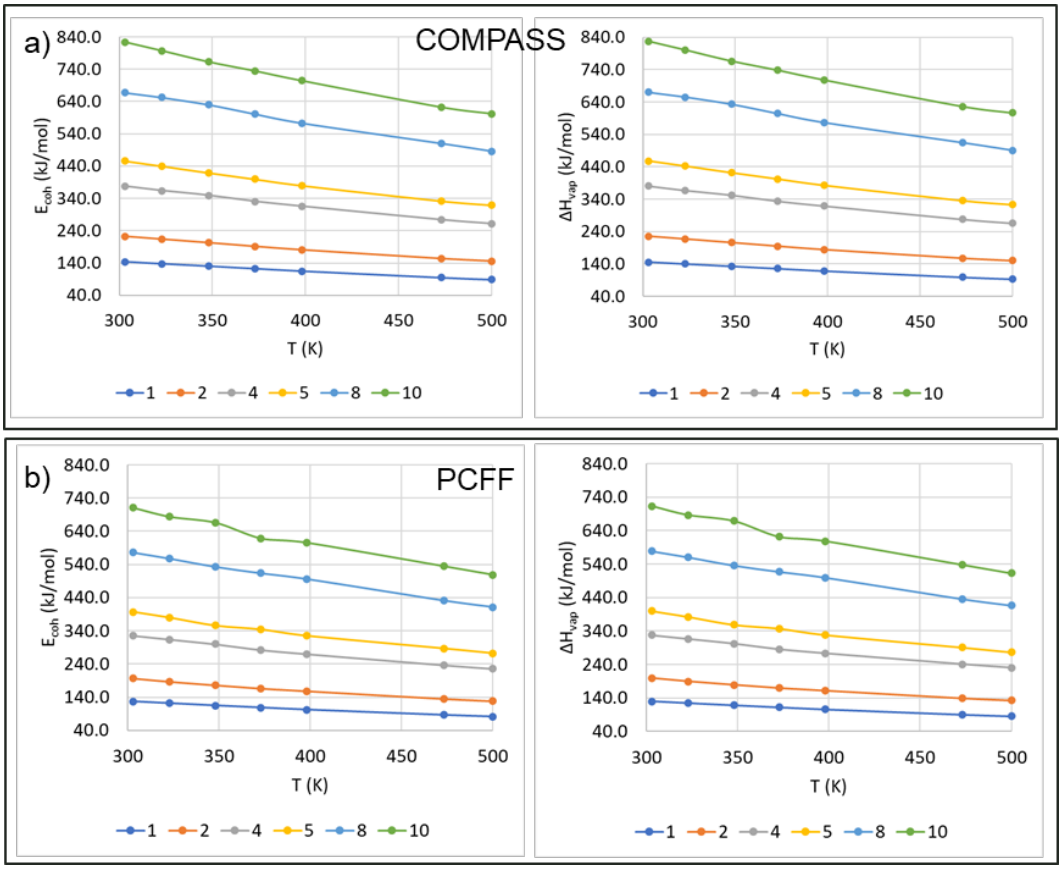

Fig. 6 COMPASS- and PCFF-based $E_{coh}(T)$ and $\Delta H_v(T)$ estimates for HO–(EODT)$_n$–OH (n = 1, 2, 4, 5, 8, 10)

Table 3 $\Delta_f H_g(298)$, $\Delta H_v(298)$, and $\Delta_f H_c(298)$ estimates for HO–(EODT)$_n$–OH systems

n	M	$\Delta_f H_g(298)$[a]		$\Delta H_{vap}(298)$[a]		$\Delta_f H_c(298)$[a]		$\Delta_f H_c(298)$[b]	
	g/mol	kJ/mol	kJ/kg	kJ/mol	kJ/kg	kJ/mol	kJ/kg	kJ/kg	SD
1	304.2	–162.6	–534.5	145.8	479.0	–308.4	–1013.5	. . .	. . .
2	574.5	43.4	75.5	225.4	392.1	–182.0	–316.6	. . .	. . .
4	1114.9	391.1	350.8	380.0	340.6	11.1	10.2	. . .	. . .
5	1385.2	534.7	386.0	457.8	330.3	76.9	55.7	223[c]	113[c]
8	2195.9	1117.5	508.9	669.8	304.8	447.7	204.1	–142[d]	356[d]
10	2736.4	1490.1	544.6	826.7	301.9	663.4	242.7	–236[e]	627[e]

[a] Current work. Details of the computation of $\Delta_f H_g(298)$ are provided in the Appendix. [b] Mean values and standard deviations (SDs) of $\Delta_f H_c(298)$ data for "HTPB" that was aggregated by Thomas and Peterson (2022). [c] Estimates for HTPB based on group contribution methods. [d] Values for HTPB based on data from open literature sources. [e] Values for HTPB based on data from thermochemical databases.

Table 3 also summarizes the QM-ESM-based $\Delta_f H_g(298)$ estimates as well as the $\Delta_f H_c(298)$ estimates produced by subtracting the corresponding $\Delta H_v(298)$ estimate from them. Focusing on the results produced for the HO–(EODT)$_8$–OH and HO–(EODT)$_{10}$–OH systems, whose chains are similar in length to those in R45M, we observed that the predictions generated on this basis were somewhat higher than the mean values of data—presumably measured—that was aggregated by Thomas and Petersen (2022). Given that the modeled systems had no cross-linking, which would presumably lower their enthalpy, it was our expectation that the estimates would be somewhat high relative to measurement-based values for actual R45M samples. That bias notwithstanding, the estimates fell within the uncertainty of the aggregated data as represented by their SDs. In addition, the MD-based $\Delta_f H_c(T)$ estimates were in good agreement with estimates produced by group contribution methods, lending credence to the latter. (Although QM-ESM-MD-based $\Delta_f H_c(T)$ estimates are far more expensive to obtain than estimates based on group contribution methods, they afford the potential for producing estimates for blends that group contribution methods cannot match.)

As a final check of the validity of the $\Delta_f H_c(T)$ predictions, we fit second-order polynomials to the predictions generated for the HO–(EODT)$_8$–OH and HO–(EODT)$_{10}$–OH systems

$$\Delta_f H_c(T) = a + bT + cT^2 \tag{14}$$

where a, b, and c were constants, and took their derivatives with respect to T to produce predictions for R45M's heat capacity (c_p). Predictions are compared to measured values in Fig. 7. As shown, the predictions were within 10% of measured values over the temperature range considered, with the increase in c_p with T being

reasonably well reproduced. As such, these results further demonstrated the potential value of this approach as a screening or design tool for notional EM ingredients.

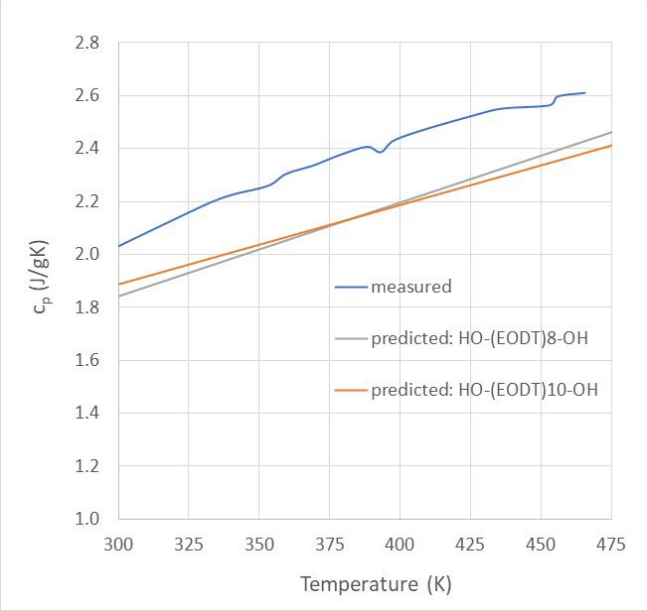

Fig. 7 Comparison of measured and predicted $c_P(T)$ values

4.3 Transport Properties

Figure 8 shows MSD(t) trajectories for c3= atom types obtained from COMPASS-based simulations of HO–EODT–OH and HO–$(EODT)_{10}$–OH systems at 303 and 500 K. For the HO–EODT–OH systems, t_d values were 20 ns, while for the HO–$(EODT)_{10}$–OH systems they were 40 ns. The square root of the MSDs at the end of the simulations indicated the average distance traveled by those atom types. At 303 K those in OH–EODT–OH chains traveled on average approximately 11 Å while at 500 K they traveled on average approximately 140 Å. In contrast, c3= atom types in HO–$(EODT)_{10}$–OH chains took 40 ns to travel on average approximately 12 Å at 303 K and approximately 45 Å at 500 K.

As noted in Section 3.1, the simulation data that were employed to derive D estimates corresponded to the temporal interval in the range $0.25t_d \leq t \leq 0.50\ t_d$ ($t_0 \leq t \leq t_{max}$). As indicated by the comparisons in Fig. 8, the MSD(t) trajectories produced by the HO–EODT–OH simulations were much more tightly grouped than those produced by the HO–$(EODT)_{10}$–OH simulations, even though the latter had longer run times. Exemplifying the need to average results for multiple independent simulations, it appeared to us that 10 was sufficient for that purpose.

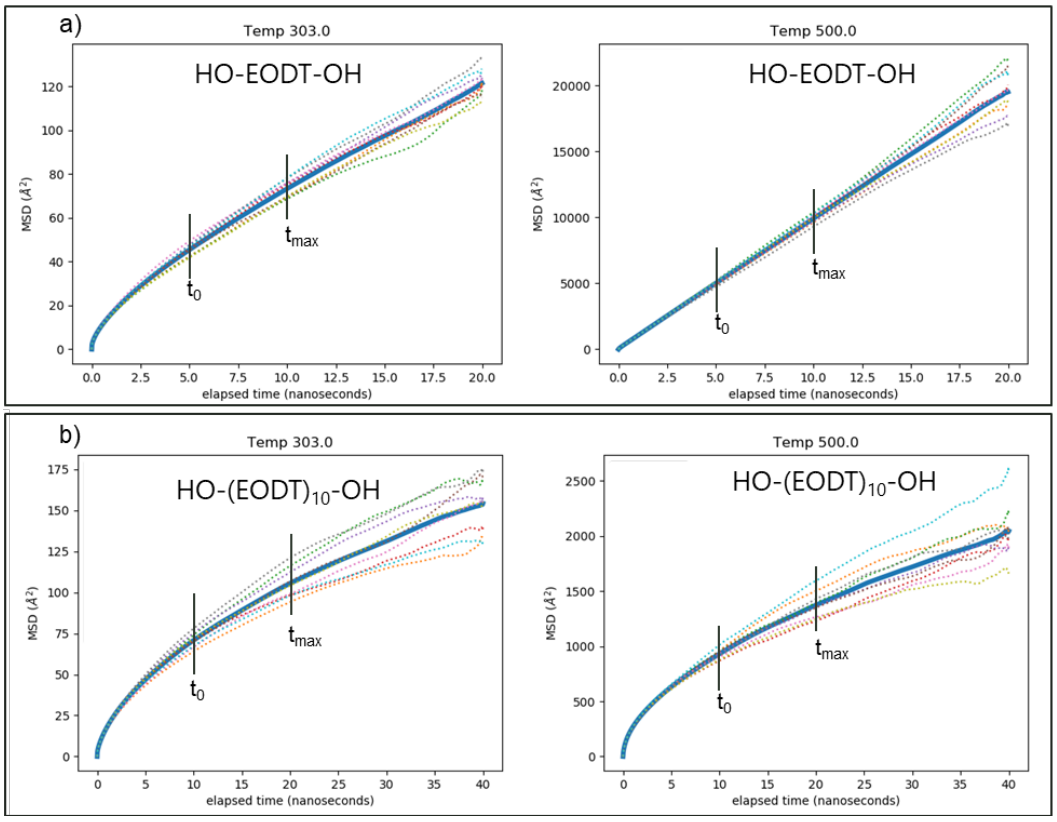

Fig. 8 COMPASS-based MSD(t) trajectories for a) HO–EODT–OH and b) HO–(EODT)$_{10}$–OH at 303 and 500 K. Curves were obtained by tracking all c3= atom types in the simulation cells. The $t_0 \leq t \leq t_{max}$ ranges employed to compute the $D(T)$ estimates are indicated.

Table 4 compares the average of the $\sqrt{\text{MSD}(t_d) - \text{MSD}(0)}$ values produced for all the HO–(EODT)$_n$–OH systems modeled in this study as a function of force-field type and temperature. Trends were as expected, with values at a given temperature decreasing with increase in n and values for a given n increasing with an increase in temperature. For a given n and T, PCFF-based estimates tended to be somewhat higher than COMPASS-based estimates. This difference can be rationalized by noting that the PCFF-based simulations produced lower ρ predictions.

Table 4 also provides the values of n' obtained by fitting Eq. 11 to ln[MSD(t)] versus ln(t) data for $0.25t_d \leq t \leq 0.5t_d$. The results suggested the adequacy of the t_d values chosen for the simulations.

Table 4 Square root of mean squared displacements ([MSD]$^{1/2}$) and *n*' as a function of oligomer size and temperature

Monomers/ oligomer (*n*)	t_d (s)	T (K)	COMPASS [MSD]$^{1/2a}$ (Å)	*n*'^{b}	PCFF [MSD]$^{1/2a}$ (Å)	*n*'^{b}
1	20	303	10.6	1.00	20.2	1.01
		323	17.2	1.00	32.3	1.00
		348	29.7	1.00	47.1	1.00
		373	45.2	1.00	64.5	1.00
		398	63.6	1.00	83.0	1.00
		473	121.3	1.00	137.8	1.00
		500	139.7	1.00	158.9	1.00
2	20	303	10.3	1.01	16.9	1.01
		323	14.8	1.01	22.8	1.01
		348	22.8	1.01	32.1	1.00
		373	32.6	1.00	44.9	1.00
		398	43.1	1.00	54.8	1.00
		473	79.9	1.00	89.9	1.00
		500	94.3	1.00	106.9	1.00
4	20	303	10.0	1.01	15.0	1.01
		323	13.8	1.01	18.8	1.00
		348	19.2	1.01	25.6	1.00
		373	24.3	1.01	31.4	1.01
		398	30.5	1.01	38.0	1.01
		473	52.1	1.00	57.7	1.00
		500	57.3	1.00	69.8	1.00
5	40	303	12.3	1.01	17.0	1.01
		323	17.0	1.01	22.2	1.02
		348	22.3	1.01	29.5	1.01
		373	29.7	1.00	35.5	1.01
		398	38.3	1.00	43.1	1.02
		473	59.3	1.00	70.7	1.00
		500	69.9	1.00	88.5	1.00
8	40	303	12.2	1.01	17.0	1.01
		323	16.0	1.01	21.3	1.01
		348	21.2	1.01	26.2	1.02
		373	25.5	1.01	31.3	1.01
		398	30.6	1.01	36.6	1.01
		473	45.2	1.01	49.8	1.01
		500	53.7	1.01	60.2	1.00

Table 4 Square root of mean squared displacements ([MSD]$^{1/2}$) and *n*' as a function of oligomer size and temperature (continued)

monomers/ oligomer (*n*)	t_d (s)	T (K)	COMPASS [MSD]$^{1/2a}$ (Å)	*n*'[b]	PCFF MSD]$^{1/2a}$ (Å)	*n*'[b]
10	40	303	12.2	1.01	16.3	1.01
		323	15.5	1.02	20.8	1.01
		348	20.1	1.02	25.2	1.02
		373	24.3	1.01	30.7	1.00
		398	28.6	1.01	33.5	1.01
		473	41.2	1.01	49.2	1.01
		500	45.0	1.01	49.7	1.01

[a] Mean of [MSD(t_d) – MSD(0)]$^{1/2}$ values from 10 simulations obtained by tracking c3= (COMPASS) and c=2 (PCFF) atom types. [b] Exponents (*n*') obtained by fitting Eq. 11 to ln[MSD(*t*)] vs. ln(*t*) data for $t_0 \le t \le t_{max}$.

Table 5 presents the *D* estimates produced for each of the HO–(EODT)$_n$–OH systems modeled in this study as a function of force-field type and temperature. Consistent with the results presented in Table 4, reductions in *D* with decrease in *T* and increase in *n* were to be expected. Table 5 also presents the limited number of measurement-based *D* values we were able to find in the open literature that bear on the merit of these estimates. Reported by Pearson et al. for polyethylene (PE) (1987) and hydrogenated polybutadiene (hPBD) (1994) with nominal *M* values similar to some of the *n*-omers modeled in this study, they suggested the validities of the estimates obtained for temperatures near 443 K.

Table 5 COMPASS- and PCFF-based *D*(*T*) estimates as a function of oligomer size

Monomers/ oligomer (*n*)	T (K)	COMPASS *D*(cm^2/s)	COMPASS ln[*D*]	PCFF *D*(cm^2/s)	PCFF ln[*D*]	Measured[a] *D*(cm^2/s)
1	303	9.3E-08	–16.2	3.0E-07	–15.0	
M = 304	323	2.5E-07	–15.2	8.0E-07	–14.0	
	348	7.0E-07	–14.2	1.8E-06	–13.2	
	373	1.7E-06	–13.3	3.5E-06	–12.6	
	398	3.4E-06	–12.6	5.6E-06	–12.1	
	473	1.2E-05	–11.3	1.6E-05	–11.0	
	500	1.6E-05	–11.0	2.2E-05	–10.7	
2	303	8.5E-08	–16.3	2.0E-07	–15.4	
M = 574	323	1.7E-07	–15.6	4.0E-07	–14.7	
	348	3.9E-07	–14.7	8.0E-07	–14.0	
	373	8.5E-07	–14.0	1.6E-06	–13.3	7E-07[b]
	398	1.4E-06	–13.5	2.4E-06	–12.9	
	448					5.4E-06[c]; 3.5E-06[d]
	473	5.2E-06	–12.2	6.8E-06	–11.9	
	500	7.3E-06	–11.8	9.6E-06	–11.6	

Table 5 COMPASS- and PCFF-based $D(T)$ estimates as a function of oligomer size (continued)

Monomers/ oligomer (n)	T (K)	COMPASS D(cm²/s)	COMPASS ln[D]	PCFF D(cm²/s)	PCFF ln[D]	Measured[a] D(cm²/s)
4	303	8.2E-08	–16.3	2.0E-07	–15.4	
M = 1115	323	1.5E-07	–15.7	3.0E-07	–15.0	
	348	2.8E-07	–15.1	5.0E-07	–14.5	
	373	4.7E-07	–14.6	7.0E-07	–14.2	
	398	6.9E-07	–14.2	1.1E-06	–13.7	
	448					2E-06[e]; 1.4E-06[f]
	473	2.0E-06	–13.1	2.6E-06	–12.9	
	500	2.5E-06	–12.9	3.8E-06	–12.5	
5	303	5.4E-08	–16.7	1.0E-07	–16.1	
M = 1385	323	1.1E-07	–16.0	2.0E-07	–15.4	
	348	1.9E-07	–15.5	3.0E-07	–15.0	
	373	3.3E-07	–14.9	5.0E-07	–14.5	
	398	5.7E-07	–14.4	7.0E-07	–14.2	
	448					
	473	1.4E-06	–13.5	2.1E-06	–13.1	
	500	1.9E-06	–13.2	2.9E-06	–12.8	
8	303	5.7E-08	–16.7	1.0E-07	–16.1	
M = 2196	323	9.9E-08	–16.1	2.0E-07	–15.4	
	348	1.6E-07	–15.7	3.0E-07	–15.0	
	373	2.5E-07	–15.2	4.0E-07	–14.7	
	398	3.6E-07	–14.8	5.0E-07	–14.5	
	448					4E-7[g]
	473	7.5E-07	–14.1	9.0E-07	–13.9	
	500	1.1E-06	–13.8	1.4E-06	–13.5	
10	303	5.8E-08	–16.7	1.0E-07	–16.1	
M = 2736	323	8.7E-08	–16.3	2.0E-07	–15.4	
	348	1.4E-07	–15.8	2.0E-07	–15.4	
	373	2.0E-07	–15.4	3.0E-07	–15.0	9E-08[h]
	398	3.1E-07	–15.0	4.0E-07	–14.7	
	448					4E-07[g]; 1.5E-07[i]
	473	6.3E-07	–14.3	9.0E-07	–13.9	
	500	7.3E-07	–14.1	9.0E-07	–13.9	

[a] PE = polyethylene; PBD = polybutadiene; hPBD = hydrogenated polybutadiene. [b] PBD: M = 690 g/mol (Fleischer and Appel 1995). [c] PE: M = 590 g/mol (Pearson et al. 1987). [d] PE: M = 695 g/mol (Pearson et al. 1987). [e] hPBD: M = 1050 amu (Pearson et al. 1994). [f] PE: M = 1280 amu (Pearson et al. 1987). [g] hPBD: M = 2510 amu (Pearson et al. 1994). [h] PBD: M = 2820 g/mol (Fleischer and Appel 1995). [i] PE: M = 3310 amu (Pearson et al. 1987).

Unable to find in the open literature any measured D values for "R45M-like" polymers with $M \leq 4{,}000$ g/mol at temperatures from 303 to 410 K, we sought to validate the $D(T)$ estimates by converting them to $\eta(T)$ estimates for which we had measured values. However, the agreement between measured values and estimates produced based on Eq. 5 proved to be poor.

Investigating further, we noted that Pearson et al. (1987, 1994) observed that the D and η values they measured for PE and hPBD systems with M values less than 4,000 g/mol conformed to the Rouse (1953) model's prediction for their product,

$$\eta(T)D(T) = \frac{\rho(T)RT\langle R_G^2\rangle}{6M} \tag{15}$$

where $\langle R_G^2\rangle$ is the mean square of the radius of gyration. For hPBD systems, they found the substitution into Eq. 15 of η, ρ, and D values for $M \leq 4{,}000$ g/mol polymers at 443 K yielded $\langle R_g^2\rangle/M$ values similar to the average of values reported by Horton et al. (1989) and Boothroyd et al. (1991) (1.97×10^{-17} cm^{2}mol/g). Since our D estimates at temperatures bounding 443 K were similar to Pearson et al.'s measurement-based D values (as a function of M) and the Rouse model would therefore produce η estimates similar to their measurement-based η values, we sought more details about it.

Our first impression of the Rouse model was that it was a simple variation of the Stokes–Einstein equation (Eq. 5) that offered an alternate physical interpretation for A'. However, further investigation revealed that, unlike A', $\langle R_G^2\rangle$ has the potential to be temperature dependent. (This was not obvious from Pearson et al.'s two studies because they only measured D and η values at one temperature: 443 K.) Indeed, $\langle R_G^2\rangle$ values are expected to increase with a decrease in temperature (Boothroyd et al. 1991).

Finding the shortcoming of our approach to converting $D(T)$ values into $\eta(T)$ values for polymers, we sought $\langle R_g^2\rangle/M$ values in the open literature that could be used for that purpose but could not find any. As an alternative, we simply combined the $\eta(T)$ values we had measured with the MD-based estimates for $D(T)$ and $\rho(T)$ to establish what $\sqrt{\langle R_g^2\rangle}$ values were needed to obtain agreement between the measured $\eta(T)$ values and the $D(T)$ predictions for HO–(EODT)$_{10}$–OH. The results are shown in Fig. 9. Consistent with Boothroyd et al.'s (1991) values at the high end of the temperature range and increasing with decrease in temperature, but not to physically unrealistic values, they do not appear unreasonable to us.

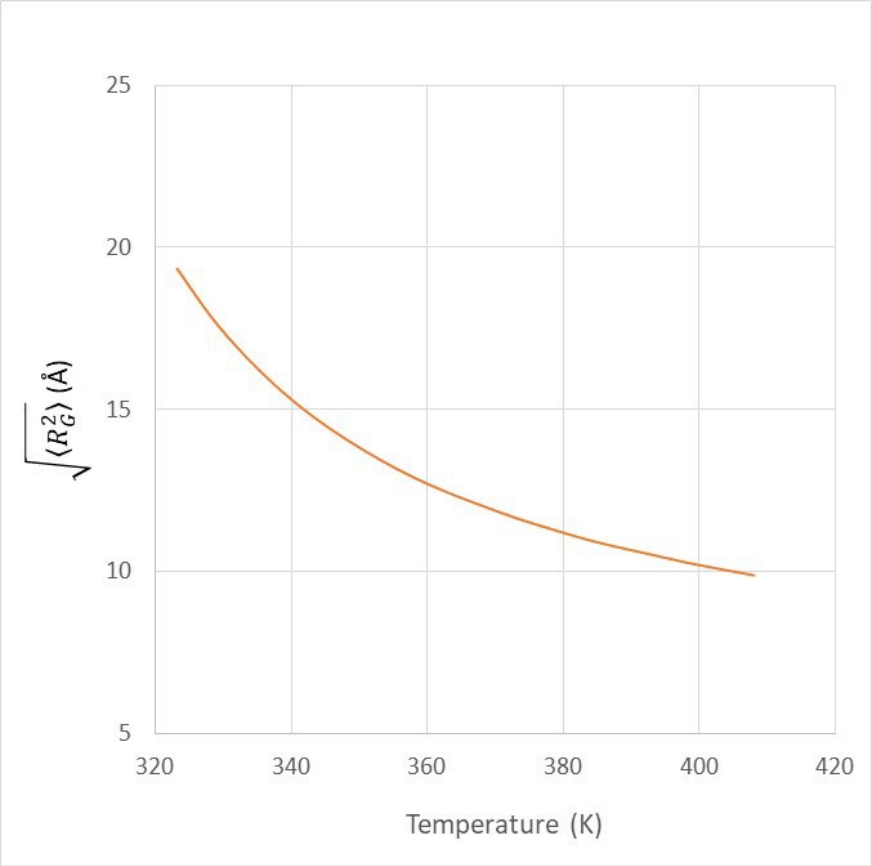

Fig. 9 $\sqrt{\langle R_G^2 \rangle}$ of HO–(EODT)$_{10}$–OH as a function of temperature derived from COMPASS-based $D(T)$ predictions and measured $\eta(T)$ values

4.4 Probability Function Parameterization

At the start of this study, we appreciated that there were qualitative differences between the dynamics of the self-diffusion of molecules that would be classified as solvents and those that would be classified as polymers. However, given that both were formulated in terms of "jumping units" and that the formulae expressing their temperature dependence had identical exponential functional forms, we assumed that Eq. 2 was the appropriate basis for parameterizing $P\left(\hat{V}_{hfv}(T)\right)$ for both cases. Moreover, we had also learned that MD-based D predictions are in general easier to obtain and more reliable than MD-based η predictions. Therefore, it was logical to generate MD-based D predictions to parameterize $P\left(\hat{V}_{hfv}(T)\right)$ for R45M.

Discovering that the theoretical foundation for this approach was not as firmly established as we had thought, we searched the open literature for a theory (comparable to FVT for solvents) that directly connected η with the "free-space"

of "polymers" that was demonstrated empirically by Doolittle (1951).[*] We could not find one. Therefore, unlike solvents, where variations of the Stokes–Einstein relationship between η and D (e.g., Dullien 1972) are applicable and directly connect η with the $\hat{V}_{hfv}$ that we believe is necessary for a reaction to occur *and* prevented from reversing, that connection has to be taken more on faith for the case of R45M. However, to the extent that $D(T)$ estimates for polymers *are* related to diffusive jumps associated with $\hat{V}_{hfv}$, we were not ready to dismiss their potential to be a basis for parameterizing $P\left(\hat{V}_{hfv}(T)\right)$. Therefore, we decided to simply compare the $P\left(\hat{V}_{hfv}(T)\right)$ parameterizations produced by fitting $\ln(A) - [-B/(T - T_0)]$ to both the COMPASS-based $D(T)$ predictions for HO–$(EODT)_{10}$–OH and to the measured $\eta(T)$ values for R45M.

Figure 10 compares the two data sets and lists the values of B and T_0 that were derived from them. While the discrepancies might be considered large, none of the values appear completely physically unrealistic to us. (To the extent we expect T_0 to correspond to R45M's T_g, the 78-K value derived on the basis of the $D(T)$ predictions does appear low.) Moreover, as shown in Fig. 11, in the temperature range of interest (300–750 K), the parameter sets produce similar $P\left(\hat{V}_{hfv}(T)\right)$ values. Therefore, to the extent we are simply trying to establish a rational basis for adjusting k_g^i to estimate k_c^i, and would be satisfied to get within an order of magnitude, the use of MD-based $D(T)$ predictions for this purpose appears to be warranted.

[*] Per the Web of Science, Doolittle's paper has been cited more than 1,600 times; therefore, there is little question as to its merit and relevance.

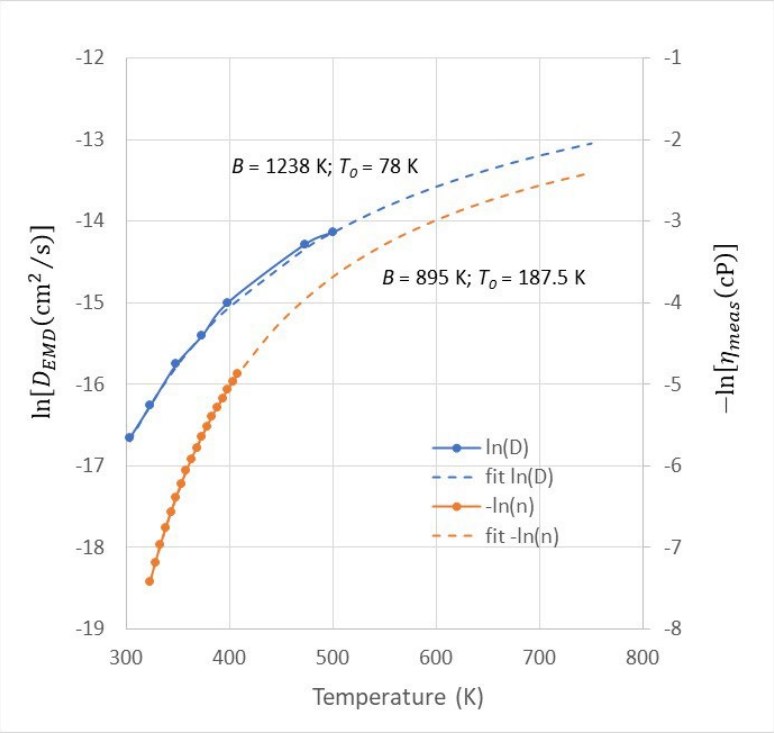

Fig. 10 Comparison of COMPASS-based ln(D) predictions and measured -ln(η) values as a function of temperature. Fits of $\ln(A) - [-B/(T - T_0)]$ to the data are also shown.

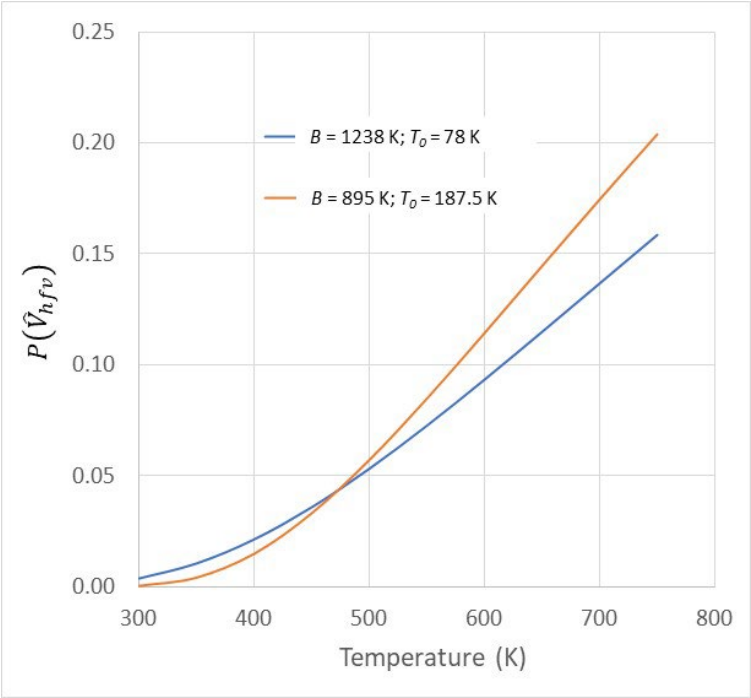

Fig. 11 Comparison of $P\left(\hat{V}_{hfv}(T)\right)$ values based on fits to COMPASS-based $D(T)$ predictions (B = 1238 K; T_0 = 78 K) and measured $\eta(T)$ values (B = 895 K; T_0 = 187.5 K)

5. Conclusion

Predictions for physical properties of amorphous R45M that are needed to model its pyrolysis and deflagration were produced via MD simulations of HO–(EODT)$_n$–OH systems. Properties of interest included $\rho(T)$, $\Delta H_v(T)$, and $D(T)$. The $\Delta H_v(T)$ estimates derived from $E_{COH}(T)$ estimates for the systems were combined with $\Delta_f H_g(T)$ estimates derived from QM-ESM-based results for their gas-phase analogs to produce $\Delta_f H_c(T)$ estimates. The $\Delta_f H_c(T)$ estimates for HO–(EODT)$_8$–OH and HO–(EODT)$_{10}$–OH were in reasonable agreement with a recently published aggregation of such values. In addition, $c_p(T)$ estimates produced by taking the derivative of the $\Delta_f H_c(T)$ estimates with respect to T were in reasonable agreement with values measured by us. Relevant to predicting the linear burning rate of R45M, these data will find application in modeling R45M's deflagration in both opposed-flow burner experiments and solid fuel ramjet combustors.

Targeting the parameterization of $P\left(\hat{V}_{hfv}(T)\right)$ for R45M, $D(T)$ estimates for HO–(EODT)$_n$–OH systems were derived from MD-generated MSD(t) data. Estimates were found to be in reasonable agreement with the limited number of relevant measurement-based values we were able to find. However, an attempt to validate the estimates based on comparisons to measured $\eta(T)$ data at the low end of the temperature range of interest, where there was effectively no validating measurement-based data, revealed (to us) that the Rouse (1953) model was a better basis for relating $D(T)$ and $\eta(T)$ for HO–(EODT)$_8$–OH and HO–(EODT)$_{10}$–OH than a "simple" Stokes–Einstein-based relationship. Moreover, it led us to appreciate for the first time that the transport property of *polymers* that is most directly correlated with "free-space" was η, not D.

Those findings notwithstanding, we parameterized $P\left(\hat{V}_{hfv}(T)\right)$ by direct fits of its functional form to the $D(T)$ predictions and the measured $\eta(T)$ values. We found that while there was a fair amount of discrepancy between the respective B and T_0 values derived from the two data sets, none were physically unreasonable. Moreover, the $P\left(\hat{V}_{hfv}(T)\right)$ values produced by the two (B, T_0) sets were similar in the temperature range of interest. Therefore, to the extent our objective was to establish a rational basis for adjusting k_g^i to estimate k_c^i, and we would be satisfied to get k_c^i values to within an order of magnitude of their actual value, we believe the use of either basis for parameterizing $P\left(\hat{V}_{hfv}(T)\right)$ merits consideration.

6. References

Abou-Rachid H, Lussier L-S, Ringuette S, Lafleur-Lambert X, Jaidann M, Brisson J. On the correlation between miscibility and solubility properties of energetic plasticizers/polymer blends: modeling and simulation studies. Propellants, Explosives, and Pyrotechnics. 2008;33:301–310.

Armado JC, Ross PG, Murakami LMS, Dutra JCN. Properties of hydroxyl-terminal polybutadiene (HTPB) and it use as a liner and binder for composite propellants: a review of recent advances. Propellants, Explosives, Pyrotechnics. 2022;47:e202100283.

Baboul AG, Curtiss LA, Redfern PC, Raghavachari K. Gaussian-3 theory using density functional geometries and zero-point energies. Journal of Chemical Physics. 1999;110:7650.

Barton AFM. CRC handbook of solubility parameters and other cohesion parameters. 2nd Ed. CRC Press; 1991, p. 739.

Becke AD. Density-functional thermochemistry. III. The role of exact exchange. Journal of Chemical Physics. 1993;98:5648–5652.

Becke AD. Density-functional thermochemistry. IV. A new dynamical correlation functional and implications for exact-exchange mixing. Journal of Chemical Physics. 1996;104:1040.

Boothroyd AT, Rennie AR, Boothroyd CB. Direct measurement of the temperature dependence of the unperturbed dimensions of a polymer. Europhysics Letters. 1991;15:715–719.

Bunte SW, Sun H. Molecular modeling of energetic materials: the parameterization and validation of nitrate esters in the COMPASS force field. The Journal of Physical Chemistry B. 2000;104:2477–2489.

Chen CC, Anderson WR, McQuaid MJ. Computationally based predictions for the burning rates and flame structure of nitroglycerin doped with various small molecules. Army Research Laboratory (US); 2019. Report No.: ARL-TR-8721.

Chen CC, McQuaid MJ. Thermochemical and kinetic studies of the pyrolysis of hydroxyl-terminated polybutadiene (HTPB). Presented at the 43rd JANNAF Combustion Subcommittee Meeting; 2009 Dec 7–11.

Chen CC, McQuaid MJ. A skeletal finite-rate chemical kinetics mechanism for modeling HTPB-air combustion in a gun-launched solid-fuel ramjet combustor. Army Research Laboratory (US); 2020 Jan. Report No.: ARL-TR-8891.

Cohen MH, Turnbull D. Molecular transport in liquids and glasses. Journal of Chemical Physics. 1959;31:1164–1169.

Doolittle AK. Studies in Newtonian flow. II. The dependence of the viscosity of liquids on free-space. Journal of Applied Physics. 1951;22:1471–1475.

Dossi E, Earnshaw J, Ellison L, Dos Santos GR, Cavaye H, Cleaver DJ. Understanding and controlling the glass transition of HTPB oligomers. Polymer Chemistry. 2021;12:2606–2617. doi: 10.1039/d1py00233c.

Dullien FAL. Predictive equations for self-diffusion in liquids: a different approach. AlChE Journal. 1972;18:62–70.

Eroglu MS. Characterization of network structure of hydroxyl terminated poly(butadiene) elastomers prepared by different reactive systems. Journal of Applied Polymer Science. 1998;70:1129–1135.

Fleischer G, Appel M. Chain length and temperature dependence of the self-diffusion of polyisoprene and polybutadiene in the melt. Macromolecules 1995;28:7281–7283.

Frisch MJ, Trucks GW, Schlegel HB, Scuseria GE, Robb MA, Cheeseman JR, Scalmani G, Barone V, Petersson GA, Nakatsuji H, et al. Gaussian 16, revision C.01; Gaussian, Inc; 2016.

Horton JC, Squires GL, Boothroyd AT, Fetter LJ, Rennie AR, Glinka CJ, Robinson RA. Small-angle neutron-scattering from star-branched polymers in the molten state. Macromolecules. 1989;681.

In ‘t Veld PJ, Rutledge GC. Temperature-dependent elasticity of a semicrystalline interphase composed of freely rotating chains. Macromolecules. 2003;36:7358–65. doi: 10.1021/ma0346658.

Jabez I, Das U, Manivannan, R, Sarat A. Influence of HTPB prepolymer on achieved properties of composite solid propellant. High Performance Polymers. 2019;31:095400831983046. doi: 10.1177/0954008319830468.

Kempfer K, Devémy J, Dequidt A, Couty M, Malfreyt P. Realistic coarse-grain model of cis-1,4-polybutadiene: from chemistry to rheology. Macromolecules. 2019;52:2736–47. doi: 10.1021/acs.macromol.8b02750.

Lee S, Choi JH, Hong I-K, Lee JW. Curing behavior of polyurethane as a binder for polymer-bonded explosives. Journal of Industrial and Engineering Chemistry. 2015;21:980–85. doi: 10.1016/j.jiec.2014.05.004.

Maginn EJ, Messerly RA, Carlson DJ, Roe DR, Elliot JR. Best practices for computing transport properties 1. Self-diffusivity and viscosity from equilibrium molecular dynamics. Living Journal of Computational Molecular Science. 2019;1:6324–6324.

Mahanta AK. HTPB-polyurethane: a versatile fuel binder for composite solid propellant. Ed. Pathak DD. ED1 - Fahmina Zafar ED2 - Eram Sharmin, Ch. 11. Rijeka: IntechOpen, 2012. doi: 10.5772/47995.

McQuaid MJ. Modeling the combustion of opposed flows of butadiene and air: A skeletal finite-rate chemical kinetics mechanism derived from the San Diego mechanism and regression rate predictions for hydroxyl-terminated polybutadiene-air systems. Army Research Laboratory (US); 2020. Report No.: ARL-TR-8918.

McQuaid MJ, Chen CC, Veals JD, Yeh IC. Detailed finite-rate chemical kinetics-based modeling of the decomposition of nitroglycerin in systems comprising liquid and gas phases. Proc. of the 43rd JANNAF Propellant and Explosives Development and Characterization Subcommittee Meeting 2021.

McQuaid MJ, Sun H, and Rigby D. Development and validation of COMPASS force field parameters for molecules with aliphatic azide chains. Journal of Computational Chemistry. 2004;25:61–71. doi: 10.1002/jcc.10316.

McQuaid MJ, Veals JD, Yeh IC, Chen CC. The development of detailed finite-rate chemical kinetics mechanisms for modeling decomposition in condensed phases. Part 2. The parameterization of free volume theory for liquid nitrate esters. Proc. of the 50th JANNAF Combustion Subcommittee Meeting 2020.

McQuaid MJ, Chen CC, Stone CP, Veals JD. On modeling the pyrolysis of hydroxyl-terminated polybutadiene (HTPB) type R45M at temperatures in the range 465–600 °C. Army Research Laboratory (US); 2023. Report No.: ARL-TR-9681.

Montgomery JA, Frisch MJ, Ochterski JW, Petersson GA. A complete basis set model chemistry. VII. Use of minimum population localization method. Journal of Chemical Physics. 2000;112:6532.

Muthiah RM, Krishnamurthy VN, Gupta BR. Rheology of HTPB propellant. 1. Effect of solid loading, oxidizer particle size, and aluminum content. Journal of Applied Polymer Science. 1992;44:2043–2052.

Pearson DS, Ver Strate G, von Meerwall E, Schilling FC. Viscosity and self-diffusion of linear polyethylene. Macromolecules. 1987;20:1133–1141.

Pearson DS, Fetters LJ, Graessley WW, Ver Strate G, von Meerwall E. Viscosity and self-diffusion of hydrogenated polybutadiene. Macromolecules. 1994;27:711–719.

Peterson JM. The viscosities of glycerol trinitrate and certain related glycol nitric esters. Journal of the American Chemical Society. 1930;52:3669–3676.

Rouse PE. A theory of the linear viscoelastic properties of dilute solution of coiling polymers. Journal of Chemical Physics. 1953;21:1272–1280

Sun H. Force field for computation of conformational energies, structures, and vibrational frequencies of aromatic polyesters. Journal of Computational Chemistry. 1994;15:752–768.

Sun H. COMPASS: an ab initio force-field optimized for condensed-phase applications overview with details on alkane and benzene compounds. Journal of Physical Chemistry B. 1998;102:7338–7364. doi: 10.1021/jp980939v.

Thomas JC, Petersen EL. HTPB heat of formation: literature survey, group additive estimations, and theoretical effects. AIAA Journal. 2022;60:1269–1282.

Veals JD, Yeh IC, Chen CC, Andzelm J, McQuaid MJ. Establishing and parameterizing rate coefficient functions for steps in the decomposition of nitrate esters in condensed phases: progress in developing a practical approach. Proceedings of the 41st JANNAF Propellant and Explosives Development and Characterization Subcommittee Meeting 2018.

Vrentas JS, Duda JL. Diffusion in polymer-solvent systems I. Re-examination of the free-volume theory. Journal of Polymer Science Part B. Polymer Physics. 1977a;15:403–416.

Vrentas JS, Duda JL. Diffusion in polymer-solvent systems II. A predictive theory for the dependence of diffusion coefficients on temperature, concentration, and molecular weight. Journal of Polymer Science Part B. Polymer Physics. 1977b;15:417–439.

Waring CE, Krastins G. Kinetics and mechanism of the thermal decomposition of nitroglycerin. The Journal of Physical Chemistry. 1970;74:999–1006. doi: 10.1021/j100700a007.

Yang L, Lin M, Yan L, Li L, Yi F. Molecular dynamics simulation on compatibility and the glass transition temperature of HTPB/plasticizer blends. Advanced Materials Research. 2013;718–720 doi: 10.4028/www.scientific.net/AMR.718-720.136.

Zhao Y, Truhlar DG. The M06 suite of density functionals for main group thermochemistry, thermochemical kinetics, noncovalent interactions, excited states, and transition elements: two new functionals and systematic testing of four M06-class functionals and 12 other functionals. Theoretical Chemistry Accounts. 2008;120:215–41.

Zheng G, Witek H, Bobadova-Parvanova P, Irle S, Musaev DG, Prabhakar R, Morokuma K, Lundberg M, Elstner M, Kohler C, Frauenheim T. Parameter calibration of transition-metal elements for the spin-polarized self-consistent-charge density-functional tight-binding (DFTB) method: Sc, Ti, Fe, Co and Ni. Journal of Chemical Theory and Computation. 2007;3:1349–67.

Zielinski JM, Duda JL. Predicting polymer/solvent diffusion coefficients using free-volume theory. AIChE Journal. 1992;38:405–415.

Appendix. HO–(EODT)$_n$–OH Oligomer Gas-Phase Enthalpies of Formation at 298 K

This Appendix lists gas-phase enthalpy-of-formation estimates at 298 K [$\Delta_f H_g(298)$] for HO–(EODT)$_n$–OH oligomers. They were obtained by calculating enthalpies of reaction for (hypothetical) isodesmic reactions based on results produced by quantum mechanics-based electronic structure methods (QM-ESMs). Table A-1 lists $\Delta_f H_g(298)$ estimates for species employed in the isodesmic reactions. Table A-2 lists $\Delta_f H_g(298)$ estimates for the oligomers. Of the QM-ESMs we typically employ for such purposes, the only two capable of producing results for HO–(EODT)$_8$–OH and HO(EODT)$_{10}$–OH were BHandHLYP/3-21G(d) and DFTBA. Therefore, $\Delta_f H_g(298)$ estimates derived from results produced by those models for smaller molecules were plotted versus $\Delta_f H_g(298)$ estimates produced with (generally) more reliable models to obtain a correction. The basis for the correction is shown in Fig. A-1.

Table A-1 $\Delta_f H_g$(298) estimates (in kJ/mol) for species employed in the isodesmic reactions in Table A-2

Isodesmic Reactions[a]	Model										
	b	**c**	**d**	**e**	**f**	**g**	**h**	**i**	**j**	**k**	**l**
$CH_2CHCHCH_2$ + C_2H_6 = CH_3CHCH_2 + CH_3CHCH_2	111.3	112.1	106.7	111.7	110.5	112.5	108.8	108.4	111.7	117.2	111.7
$CH_2CHCH_2CH_2CHCH_2$ + 3 C_2H_6 = 2 CH_3CHCH_2 + 2 $CH_3CH_2CH_2$	83.7	84.1	85.8	87.0	84.5	84.5	85.8	85.4	84.1	88.7	83.7
$CH_2CHCHCHCHCH_2$ + C_2H_6 + C_2H_4 = $CH_2CHCHCH_2$ + 2 CH_3CHCH_2	167.4	166.9	161.9	166.9	166.1	168.6	164.4	164.4	165.3	172.4	167.4
(E) $CH_3CHCHCH_3$ + C_2H_4 = CH_3CHCH_2 + CH_3CHCH_2	–10.0	–10.5	–9.6	–9.2	–10.0	–9.6	–10.0	–10.9	–10.0	–8.8	–10.5
(E) $CH_3CHCHCH_2CH_3$ + C_2H_6 = $CH_3CHCHCH_3$ + $CH_3CH_2CH_3$	–31.0	–30.5	–30.1	–29.7	–30.1	–30.1	–29.7	–31.0	–30.1	–29.3	–31.0
(Z) $CH_3CHCHCH_2CH_3$ + C_2H_6 = $CH_3CHCHCH_3$ + $CH_3CH_2CH_3$	–25.5	–25.1	–23.0	–24.3	–24.7	–25.1	–23.0	–24.3	–25.5	–24.7	–25.1
$CH_3CH_2CHCHCH_2CH_3$ + C_2H_6 = $CH_3CHCHCH_2CH_3$ + $CH_3CH_2CH_3$	–51.0	–51.0	–50.2	–49.8	–50.6	–50.6	–50.2	–51.5	–50.6	–50.2	–51.5
(E, E) $CH_3CHCHCHCH_2$ + C_2H_6 = $CH_3CHCHCH_3$ + CH_3CHCH_2	79.1	78.7	74.1	78.7	76.6	78.2	76.1	75.7	78.2	82.8	78.7
(E, Z) $CH_3CHCHCHCH_2$ + C_2H_6 = $CH_3CHCHCH_3$ + CH_3CHCH_2	90.8	91.2	88.7	92.0	89.1	91.2	90.0	89.5	84.1	88.7	91.2
(Z, E) $CH_3CHCHCHCH_2$ + C_2H_6 = $CH_3CHCHCH_3$ + CH_3CHCH_2	84.5	84.1	81.2	84.1	83.7	85.4	83.3	82.4	82.8	87.4	84.9
$CH_3CH_2CH_2C(CH_3)CH_2$ + 2 C_2H_6 = $(CH_3)_3CH$ + CH_3CHCH_2 + $CH_3CH_2CH_3$	–50.6	–50.6	–47.7	–46.9	–51.0	–49.4	–47.3	–48.5	–49.4	–49.0	–51.0
$CH_2CHCH_2CH_2CHCHCH_2CH_2CHCH_2$ + 4 C_2H_6 = $CH_3CH_2CHCHCH_2CH_3$ + 2 CH_3CHCH_2	115.9	115.1	118.0	119.2	115.9	116.3	118.4	118.0	115.5	120.9	114.2

[a] Target species is in bold face. Reference $\Delta_f H_g(298)$ data (in kJ/mol): C_2H_6 = –83.8 ± 0.3 (Pittam and Pilcher 1972); C_2H_4 = 52.5 ± 0.4 (Chase 1998); $CH_3CH_2CH_3$ = –104.7 ± 0.4 (Pittam and Pilcher 1972)[1]; CH_3CHCH_2 = 20.4 ± 0.7 (Furuyama et al. 1969)[2]; $(CH_3)_3CH$ = –134.2 ± 0.6 (Pittam and Pilcher 1972)[1]; CH_3CH_2OH = –234.3 ± 0.8 (Chao and Rossini 1965)[3]; [b] CBS-QB3; [c] G3MP2B3; [d] B3LYP/6-31G(2df,p); [e] MPWB95/6-31+g(d,p); [f] M062X/6-31G(2df,p); [g] M062X/6-311+G(2d,2p); [h] BHandHLYP/3-21g(d); [i] Correlated values using linear regression line in Fig. 1a; [j] DFTBA; [k] Correlated values using linear regression line in Fig. 1b; [l] Recommended value based on average of corrected BHandHLYP/3-21g(d)- and DFTBA-based values.

[1] Pittam, DA, Pilcher G. Measurements of heats of combustion by flame calorimetry. Part 8.-Methane, ethane, propane, n-butane and 2-methylpropane. Journal of the Chemical Society, Faraday Transactions 1: Physical Chemistry in Condensed Phases. 1972;68:2224–2229.

[2] Furuyama S, Golden DM, Benson SW. Thermochemistry of the gas phase equilibria i-C3H7I = C3H6 + HI, n-C3H7I = i-C3H7I, and C3H6 + 2HI = C3H8 + I2. The Journal of Chemical Thermodynamics. 1969;1:363–375.

[3] Chao J, Rossini FD. Heats of combustion, formation, and isomerization of nineteen alkanols. J Chem Eng Data. 1965;10:374–379.

Table A-2 $\Delta_f H_g$(298) estimates (in kJ/mol) for HO–(EODT)$_n$–OH oligomers

Isodesmic Reactions[a]	Model										
	b	**c**	**d**	**e**	**f**	**g**	**h**	**i**	**j**	**k**	**l**
EODT + 6 C_2H_6 = 2 $CH_3CH_2CHCHCH_2CH_3$ + 2 $CH_3CH_2CH_3$ + $CH_3CH_2CH_2C(CH_3)CH_2$	. . .	118.0	130.1	129.3	121.8	123.8	130.1	129.7	121.3	127.2	124.3
HO–EODT–OH + 2 C_2H_6 = EODT + 2 CH_3CH_2OH	. . .	. . .	–163.2	–161.1	–162.8	–162.8	–162.3	–164.0	–172.4	–176.1	–162.8
HO–(EODT)$_2$–OH + 3 C_2H_6 = EODT + HO(EODT)OH + 2 $CH_3CH_2CH_3$	. . .	. . .	43.9	36.0	. . .	. . .	44.4	42.7	27.2	29.7	40.2
HO–(EODT)$_2$–OH + 3 CH_3CHCH_2 = EODT + HO(EODT)OH + $CH_2CHCH_2CH_2CHCH_2$	. . .	. . .	42.3	32.6	. . .	. . .	42.3	0.0	26.8	29.3	0.0
HO–(EODT)$_4$–OH + 4 CH_3CHCH_2 + $CH_3CHCHCH_3$ = 3 EODT + HO–EODT–OH + $CH_2CHCH_2CH_2CHCH_2$ + $CH_2CHCH_2CH_2CHCHCH_2CH_2CHCH_2$	. . .	. . .	. . .	. . .	. . .	. . .	391.2	392.5	364.4	378.2	392.5
HO–EODT)$_5$OH + 4 CH_3CHCH_2 + 2 $CH_3CHCHCH_3$ = 4 EODT + HO–EODT–OH + 2 $CH_2CHCH_2CH_2CHCHCH_2CH_2CHCH_2$	. . .	. . .	. . .	. . .	. . .	. . .	534.7	536.8	515.9	534.3	536.8
HO–(EODT)$_8$–OH + 8 CH_3CHCH_2 + 3 $CH_3CHCHCH_3$ = 7 EODT + HO–EODT–OH + $CH_2CHCH_2CH_2CHCH_2$ + 3 $CH_2CHCH_2CH_2CHCHCH_2CH_2CHCH_2$	. . .	. . .	. . .	. . .	. . .	. . .	. . .	. . .	1080.7	1117.5	1117.5
HO–(EODT)$_{10}$–OH + 10 CH_3CHCH_2 + 4 $CH_3CHCHCH_3$ = 9 EODT + HO–EODT–OH + $CH_2CHCH_2CH_2CHCH_2$ + 4 $CH_2CHCH_2CH_2CHCHCH_2CH_2CHCH_2$	. . .	. . .	. . .	. . .	. . .	. . .	. . .	. . .	1441.4	1490.3	1490.3

[a] Target species is in bold face. Reference data (in kJ/mol): C_2H_6 = –83.8 ± 0.3 (Pittam and Pilcher 1972)[1]; C_2H_4 = 52.5 ± 0.4 (Chase 1998)[2]; $CH_3CH_2CH_3$ = –104.7 ± 0.4 (Pittam and Pilcher 1972)[1]; CH_3CHCH_2 = 20.4 ± 0.7 (Furuyama et al. 1969)[3]; $(CH_3)_3CH$ = –134.2 ± 0.6 (Pittam and Pilcher 1972)[1]; CH_3CH_2OH = –234.3 ± 0.8 (Chao and Rossini 1965)[4]; [b] CBS-QB3; [c] G3MP2B3; [d] B3LYP/6-31G(2df,p); [e] MPWB95/6-31+g(d,p); [f] M062X/6-31G(2df,p); [g] M062X/6-311+G(2d,2p); [h] BHandHLYP/3-21g(d); [i] Correlated values using linear regression line in Fig. 1a; [j] DFTBA; [k] Correlated values using linear regression line in Fig. 1b; [l] Recommended value based on average of corrected BHandHLYP/3-21g(d)- and DFTBA-based values.

[1] Pittam, DA, Pilcher G. Measurements of heats of combustion by flame calorimetry. Part 8.-Methane, ethane, propane, n-butane and 2-methylpropane. Journal of the Chemical Society, Faraday Transactions 1: Physical Chemistry in Condensed Phases. 1972;68:2224–2229.

[2] Chase MW. NIST-JANAF thermochemical tables 4th edition. Journal of Physical and Chemistry Reference Data, Monograph. 1998;9:1–1951.

[3] Furuyama S, Golden DM, Benson SW. Thermochemistry of the gas phase equilibria i-C3H7I = C3H6 + HI, n-C3H7I = i-C3H7I, and C3H6 + 2HI = C3H8 + I2. The Journal of Chemical Thermodynamics. 1969;1:363–375.

[4] Chao J, Rossini FD. Heats of combustion, formation, and isomerization of nineteen alkanols. J Chem Eng Data. 1965;10:374–379.

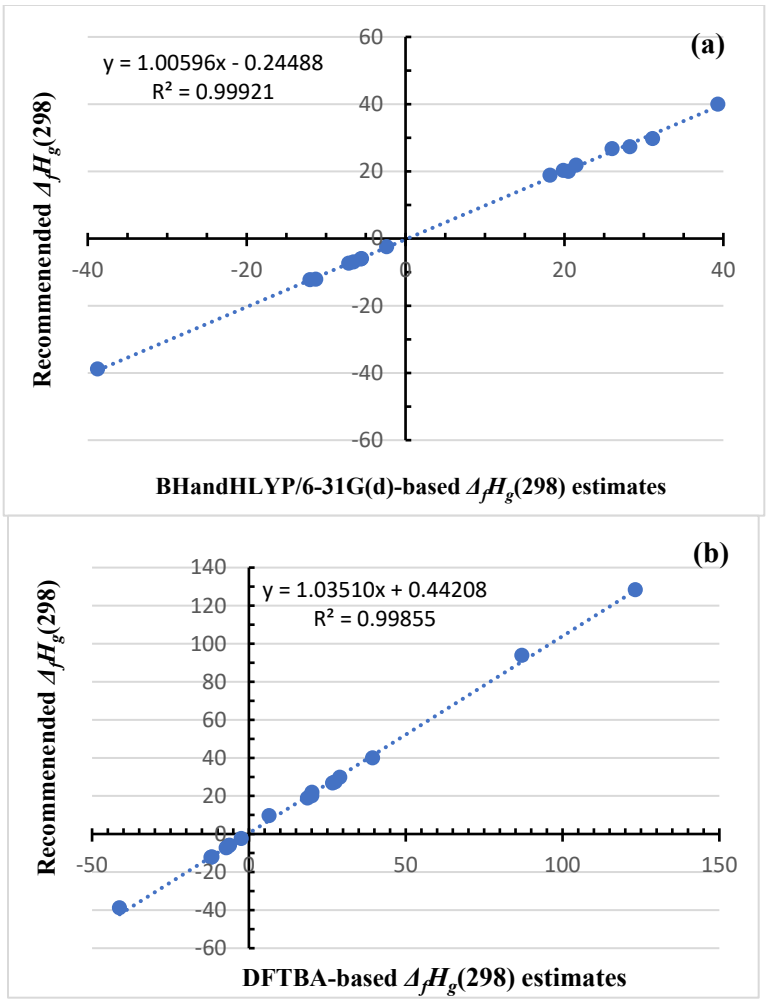

Fig. A-1 Recommended $\Delta_f H_g$(298) estimates for molecules listed in Table 1 vs. $\Delta_f H_g$(298) estimates based on (a) BHandHLYP/3-21g(d) and (b) DFTBA

List of Symbols, Abbreviations, and Acronyms

BD	butadiene
CG-DPD	coarse-grained dissipative particle dynamics
DOD	Department of Defense
EM	energetic material
EMC	Enhanced Monte Carlo
EODT	6-ethenenyl-2,8,12,16-octadecatetraene
FVT	free-volume theory
hPBD	hydrogenated polybutadiene
HR	homogeneous reactor
HTPB	hydroxyl-terminated polybutadiene
LAMMPS	Large-scale Atomic/Molecular Massively Parallel Simulator
MD	molecular dynamics
MSD	mean square displacement
M	molecular weight
NG	nitroglycerin
NPT	constant-temperature, constant-pressure ensemble
PBD	polybutadiene
PE	polyethylene
PPPM	particle–particle particle–mesh
QM-ESM	quantum mechanics-based electronic structure method

1 (PDF) DEFENSE TECHNICAL INFORMATION CTR
DTIC OCA

1 (PDF) DEVCOM ARL
FCDD RLB CI
TECH LIB

13 (PDF) DEVCOM ARL
FCDD RLA MG
I-C YEH
FCDD RLA WA
N TRIVEDI
E BYRD
B BARNES
R PESCE-RODRIGUEZ
FCDD RLA WC
M MCQUAID
C-C CHEN
C STONE
M MINNICINO
R CORNELL
M NUSCA
FCDD RLD CD
J VEALS
FCDD RLR A
J CIEZAK

2 (PDF) NAWCWD
C DENNIS
T TRAN-NGO

1 (PDF) OFFICE OF NAVAL RESEARCH
C STOLTZ

4 (PDF) US NAVAL RESEARCH LABORATORY
B BOJKO
T LOEGEL
A EPSHTEYN
CJ PFUZNER
IV SCHWEIGERT

2 (PDF) PURDUE UNIVERSITY
C GOLDENSTEIN
S SON

1 (PDF) TEXAS A&M
E PETERSEN